Journal of Nuclear Medicine, published on April 23, 2015 as doi:10.2967/jnumed.115.155176

^{64}Cu-Labeled Divalent Cystine Knot Peptide for Imaging Carotid Atherosclerotic Plaques

Lei Jiang[1, 2], Yingfeng Tu[2], Richard H. Kimura[2], Frezghi Habte[2], Hao Chen[2], Kai Cheng[2], Hongcheng Shi[1], Sanjiv Sam Gambhir[2], Zhen Cheng[2*]

1. Department of Nuclear Medicine, Zhongshan Hospital, Fudan University, Shanghai, China;
2. Molecular Imaging Program at Stanford (MIPS), Department of Radiology and Bio-X Program, Canary Center at Stanford for Cancer Early Detection, Stanford University, Stanford, CA, USA.

Running Title: Knottin for PET of Atherosclerotic Plaque

Total word counts: 4993

*Correspondence should be addressed:

Zhen Cheng, Ph.D.
Molecular Imaging Program at Stanford
Department of Radiology and Bio-X Program
Stanford University
E-mail: zcheng@stanford.edu

Abstract

The rupture of vulnerable atherosclerotic plaques that lead to stroke and myocardial infarction may be induced by macrophage infiltration, and augmented by the expression of integrin $\alpha_v\beta_3$ Indeed, atherosclerotic angiogenesis may be a promising marker of inflammation. In this study, an engineered integrin $\alpha_v\beta_3$ integrin targeting positron emission tomography (PET) probe, ^{64}Cu-NOTA-3-4A, derived from a divalent knottin miniprotein was evaluated in a mouse model for carotid atherosclerotic plaques. **Methods:** Atherosclerotic plaques in BALB/C mice, maintained on a high fat diet, were induced with streptozotocin injection and carotid artery ligation, and verified by magnetic resonance imaging (MRI). Knottin 3-4A was synthesized by solid phase peptide synthesis chemistry, and coupled to 1,4,7-triazacyclononane-1,4,7-triacetic acid (NOTA) prior to radiolabeling with ^{64}Cu. PET probe stability in mouse serum was evaluated. Mice with carotid atherosclerotic plaques were tail-vein injected with ^{64}Cu-NOTA-3-4A or ^{18}F-FDG followed by small animal PET/CT imaging at different time points. Receptor targeting specificity of the probe was verified by co-injection of c(RGDyK) administered in molar excess. Subsequently, carotid artery dissection and immunofluorescence staining were performed to evaluate target expression. **Results:** ^{64}Cu-NOTA-3-4A was synthesized in high radiochemical purity and yield, and demonstrated molecular stablilty in both PBS and mouse serum at 4 h. Small animal PET/CT showed that ^{64}Cu-NOTA-3-4A accumulated at significantly higher levels in the neovasculature of carotid atherosclerotic plaques (7.41 ± 1.44 %ID/g *vs*. 0.67 ± 0.23 %ID/g, $P<0.05$) compared to healthy or normal vessels at 1 h postinjection (p.i.). ^{18}F-FDG also accumulated in atherosclerotic lesions at 0.5 and 1 h p.i., but at lower plaque-to-normal tissue

ratios compared to ^{64}Cu-NOTA-3-4A. For example, plaque-to-normal carotid artery ratios for ^{18}F-FDG and ^{64}Cu-NOTA-3-4A at 1 h p.i. were 3.75 and 14.71 (P<0.05), respectively. Furthermore, uptake of ^{64}Cu-NOTA-3-4A in atherosclerotic plaques was effectively blocked (~90% at 1 h p.i.) by co-injection of c(RGDyK). Immunostaining confirmed integrin $\alpha_v\beta_3$ expression in both the infiltrating macrophages and the neovasculature of atherosclerotic plaques.

Conclusion: ^{64}Cu-NOTA-3-4A demonstrates specific accumulation in carotid atherosclerotic plaques where macrophage infiltration and angiogenesis are responsible for elevated integrin $\alpha_v\beta_3$ levels. Therefore, ^{64}Cu-NOTA-3-4A may demonstrate clinical utility as a PET probe for atherosclerosis imaging, or for the evaluation of therapies used to treat atherosclerosis.

Key words: Knottin, atherosclerotic plaque, $\alpha_v\beta_3$ integrin, ^{64}Cu, PET/CT

INTRODUCTION

Cardiovascular disease induced by atherosclerosis is a leading cause of death in the Western world. The majority of myocardial infarctions and sudden cardiac deaths result from the rupture of vulnerable atherosclerotic plaques *(1-4)*. Therefore, tools that detect atherosclerotic plaques are needed in the clinic. At present, several imaging modalities are used to identify atherosclerotic lesions in patients, including computed tomography angiography (CTA), magnetic resonance imaging (MRI), intravascular ultrasound (IVUS), etc. Although these imaging modalities have been able to delineate certain features of plaques, their sensitivity and specificity are relatively low *(5, 6)*. On the other hand, nuclear imaging techniques such as positron emission tomography (PET) may provide a more sensitive and quantitative route to determine the extent of cardiovascular disease *(7)*.

Inflammation is a well studied feature of atherosclerotic plaques that are at high risk of rupture *(1, 2)*. Therefore, molecular imaging of inflammation-associated-markers may be a promising tool to quantify rupture risk of plaques, and warn against further adverse cardiovascular events. The most widely studied PET probe for detection of plaque-based inflammation is ^{18}F-fluorodeoxyglucose (^{18}F-FDG) *(8, 9),* which is taken up by active macrophages so that it provides information about the extent of inflammation in atherosclerotic plaques *(10-12)*. However, ^{18}F-FDG is a nonspecific imaging probe for inflammation, because it can also accumulate in clacified structures of vessel walls, muscle tissues adjacent to the vessels as well as tissues with high metabolic rates such as the mycardium and brain. Therefore, new PET probes to image plaque-related inflammation and their propensity to rupture are needed in treating

heart disease *(13)*.

Recently, integrin $\alpha_v\beta_3$ expression in atherosclerosis has been reported to be a promising marker of vulnerable plaques *(14-16)*. Integrin $\alpha_v\beta_3$ receptors are transmembrane glycoproteins, which are highly expressed by not only activated endothelial cells of new vessels in the atherosclerotic plaques, but also activated macrophages that mediate the inflammatory process. Therefore, radiolabelled peptides such as Arg-Gly-Asparatic acid (RGD) peptide that specifically bind to $\alpha_v\beta_3$ integrin have been studied by PET imaging of atherosclerotic plaques *(13,17-20)*. For example, ^{18}F-Galacto-RGD *(13)* and ^{68}Ga-DOTA-RGD *(17)* have shown specific targeting to integrin $\alpha_v\beta_3$. However, their accumulation in atherosclerotic lesions as well as their plaque-to-normal tissue ratios are low in preclinical models. The uptake of ^{18}F-Galacto-RGD by the aorta plaque was only 0.24%ID/g at 2 h post-injection (p.i.), and the aorta-to-normal vessel wall uptake ratio was 1.3 *(13)*. The aorta plaque uptake of ^{68}Ga-DOTA-RGD was 0.90%ID/g at 1 h p.i., and aorta/heart and aorta/blood uptake ratios were 1.8 and 1.1 at 1 h p.i., respectively *(17)*. Therefore, PET probes, with higher integrin $\alpha_v\beta_3$ receptor binding affinity and specificity are needed to be of any clinical utility in management of cardiovascular disease.

Cystine knot peptides, also known as knottins, are small polypeptides that are characterized by a stable core motif formed by multiple disulfide bonds (three or four) that are interwoven into a knotted conformation, which endows these peptides with high thermal and proteolytic stability. They are relatively small (30-50 amino acids) and often made by FMOC (or BOC) solid-phase peptide synthesis. Importantly, knottins demonstrate fast blood clearance, high and specific integrin $\alpha_v\beta_3$ targeting ability, and biocompatibility. Together, these biological, chemical and

physical properties bode well for clinical imaging applications. In our previous studies, monovalent and bivalent integrin $\alpha_v\beta_3$ knottin binders have been coupled to a variety of multimodal imaging labels (radionuclides and/or fluorescent dyes) and successfully used to image $\alpha_v\beta_3$ positive tumors in small animal models *(21-28)*.

In this work, a bivalent integrin $\alpha_v\beta_3$ knottin binder 3-4A was conjugated at its N-terminus to 1,4,7-triazacyclononane-1,4,7-triacetic acid (NOTA) and radiolabeled with ^{64}Cu for PET imaging. The resulting probe was successfully used to image integrin $\alpha_v\beta_3$ expression associated with carotid atherosclerotic plaques.

MATERIALS and METHODS

General and Animal Model

All 9-fluorenylmethyloxycarbonyl (Fmoc) protected amino acids were purchased from Novabiochem/EMD Chemicals Inc. or CS Bio. c(RGDyK) peptide was purchased from Peptides International. Phosphate buffered saline (PBS, 0.01 M, pH 7.4) was obtained from Gibco/Invitrogen. All other chemicals were purchased from Fisher Scientific unless otherwise specified.

Male BALB/C mice were purchased from Charles River Laboratory. As shown in Figure 1A, carotid atherosclerotic plaques were induced in male BALB/C mice by the following protocol. Mice (n=20) were fed with a high-fat diet containing 40% kcal fat, 1.25% (by weight) cholesterol and 0.5% (by weight) sodium cholate (D12109, Research Diets, Inc.). After 4 weeks of high-fat diet, mice were rendered diabetic by administration of 7 daily intraperitoneal injection of

Streptozotocin [(STZ, 40 mg/kg in citrate buffers (0.05 mol/L, pH=4.5, Sigma Aldrich)]. At day 7 of the STZ injections, serum glucose level was measured by sampling tail vein blood and using a glucometer. If the glucose level was below 200 mg/L, animals were injected with additional STZ for 3 consecutive days. At day 14 after initiation of STZ injection, the left common carotid artery was ligated below the bifurcation with the use of 6-0 silk ligature (Ethicon) under 2% inhaled isoflurane. In sham-operated animals, the suture was put around the exposed left carotid artery but not tightened. The wound was closed by suture and the mice were allowed to recover on a warming blanket. All procedures were approved by the Administrative Panel on Laboratory Animal Care at Stanford University.

Small Animal MR Imaging

Mice (n=20) from the treatment described above were sequentially anesthetized using 2% isoflurane and placed supine in a specially designed stage with the top of its neck centered in a small, circular MRI coil. The small animal MRI scanner consisted of a superconducting magnet (Magnex Scientific) with 7.0 T field strength, a gradient (Resonance Research, Inc.) with a clear bore size of 9 cm, a maximum gradient amplitude of 770 mT/m and a maximum slew rate of 2,500 T/m/s and a General Electric console and Copley 266 amplifiers. A 15-second localizer scan was conducted first followed by a pre-scan to allow for manual gradient shimming. Then, a T1-weighted fast spin echo (FSE) sequence was obtained from the bottom of the head to the top of the chest. No contrast agents were given. This scan was approximately 5 minutes long for 30 slices and had an isotropic resolution of 20 mm. The mouse was then removed from the scanner

and allowed to recover in its cage. The small-animal MRI data were analyzed using the commercially available DICOM image viewer OsiriX (http://www.osirix-viewer.com/).

Peptide Synthesis and Folding, NOTA Conjugation and ^{64}Cu Labeling

The linear knottin 3-4A was synthesized with a CS BioCS336 instrument using Fmoc-based solid-phase peptide synthesis, and the crude peptide was deprotected and cleaved from resin as reported previously *(25)*. Linear 3-4A peptide was oxidized and folded in 4 M guanidinium chloride, 10 mM reduced glutathione, 2 mM oxidized glutathione, and 3.5 % (v/v) dimethylsulfoxide (DMSO) at pH 8.0 in ammonium bicarbonate buffer at room temperature for 1 day with gentle mixing. Folded peptide was purified on a Vydac C18 preparatory scale column and lyophilized. Purified peptide was dissolved in water, and concentration was determined by amino acid analysis (AAA Service Laboratory). Similarly, peptide purity and molecular mass were determined by analytic-scale reversed phase HPLC and MALDI-TOF-MS, respectively.

NOTA, 1-ethyl-3-[3-(dimethylamino)propyl]carbodiimide, and N-hydroxysulfono-succinimide at a molar ratio of 1:1:0.8 were mixed in water and incubated at 4 ^{o}C for 30 min (pH 5.5). 3-4A was then added to the in situ-prepared sulfosuccinimidyl ester of NOTA in a theoretic stoichiometry of 1:5 in sodium phosphate buffer (pH 8.5-9.0). The solution was reacted at 4 ^{o}C overnight, and the resulting NOTA-3-4 conjugate was purified by reversed-phase HPLC and characterized by MALDI-TOF-MS as described above. NOTA-3-4A (25 μg) was radiolabeled with ^{64}Cu by the addition of 74-111 MBq (2-3 mCi) of $^{64}CuCl_2$ (University of Wisconsin) in 0.1 N sodium acetate (pH 5.5), followed by 1 h incubation at 37 ^{o}C. The radiolabeled complex was purified by a PD-10 column (GE Healthcare Life Sciences) and eluted with PBS buffer.

In Vitro Stability

^{64}Cu-NOTA-3-4A (1.85-3.7 MBq, 50-100 μCi) was incubated in 0.5 mL of mouse serum for 4 h at 37 ^{o}C. The mixture was then treated with 0.5 mL of acetonitrile to precipitate the serum protein and centrifuged at 16,000g for 2 min. The supernatant containing greater than 95% of the radioactivity was filtered using a 0.22 μm nylon SpinX column (Corning Inc.). Greater than 99% of the radioactivity passed through this filter. In addition, ^{64}Cu-NOTA-3-4A (1.85-3.7 MBq, 50-100 μCi) was also incubated in PBS buffer for 4 h at room temperature. The samples were analyzed by radio-HPLC, and the percentage of intact peptide was determined by quantifying peaks corresponding to the intact peptide and degradation products.

Small Animal PET/CT

^{64}Cu-NOTA-3-4A. PET/CT imaging of BALB/C mice with carotid atherosclerotic plaques was performed using a small animal PET/CT scanner (Siemens Inveon). Mice (n = 4 or each group) were injected via the tail vein with approximately 3.7-5.55 MBq (100-150 μCi) of ^{64}Cu-NOTA-3-4A. At 1, 2, 4 and 24 h p.i., mice were anesthetized for imaging experiments. On the second day, the same group of mice were injected through tail vein with 2.96-3.7 MBq (80-100 μCi) of ^{64}Cu-NOTA-3-4A with or without ~330 μg of c(RGDyK) as blocking agent. At 1, 2, 4 and 24 h p.i., mice were keeping space consistent throughout (5% isoflurane for induction and 2% for maintenance in 100% O_2) for the imaging experiment.

The images were reconstructed with two-dimensional ordered-subset expectation maximization algorithm with CT-based attenuation correction. Image files were analyzed using the vendor-supplied software Inveon Research Workspace (Preclinical Solutions; Siemens

Healthcare Molecular Imaging). For each small-animal PET scan, three-dimensional (3D) regions of interest (ROIs) were drawn over the organs and tissues on decay-corrected whole-body images. The average radioactivity concentration in the ROI was obtained from the mean pixel values within the ROI volume. These data were converted to counts per milliliter per minute by using a predetermined conversion factor. The results were divided by the injected dose to obtain an image ROI derived percent injected dose per gram of tissue *(29)*.

^{18}F-FDG. Similar to ^{64}Cu-NOTA-3-4A PET/CT scan, mice models (n = 4) was also were injected via the tail vein with approximately 3.7-5.55 MBq (100-150 μCi) of ^{18}F-FDG. At 0.5 and 1 h post-injection (p.i.), mice were anesthetized for imaging experiments.

Immunofluorescence Staining

Air-dried frozen slides (10-μm thickness) of carotid tissues were fixed in ice-cold acetone and blocked by incubation with 1% PBS/BSA for 30 min to prevent unspecific binding. Immunofluorescence staining was performed using anti-integrin α_v + β_3 (CD51+CD61) polyclonal antibody (Bioss) for αvβ3 integrin with anti-CD68 antibody (Abcam) for macrophages and with anti-CD31 antibody (Abcam) for endothelial cells, respectively. Finally, sections were counterstained with 4,6-diamidino-2-phenylindole (DAPI) for visualization of cell nuclei. The slides were observed under a microscope (Axiovert 200M), and images were acquired under the same conditions and displayed at the same scale for comparison.

Statistical Analysis

The quantitative data were expressed as mean ± SD. Means were compared using the Student t test. A 95% confidence level was chosen to determine the significance between groups, with *P*

values of less than 0.05 indicating significant differences.

RESULTS

Establishment of Carotid Atherosclerotic Plaques

MRI was used to evaluate whether the carotid atherosclerotic plaques were successfully established in mouse models subjected to PET imaging protocols. Compared to the normal contralateral carotid artery, MRI revealed stenosis within the affected artery as shown on axial MRI image (Figure 1B). Moreover, a longitudinal plane of the 3D-FLASH MR images show that blood flow in the affected (left) artery was significantly decreased compared to the normal (right) carotid artery (Figure 1C). Following acquisition of MRI and PET data, mouse models were euthanized so that injured artery could be examined by bright field magnification. These anatomic images clearly show the damaged vessel wall (solid white structure) of the left artery (Figure 1D).

Preparation of ^{64}Cu-NOTA-3-4A

Linear 3-4A was synthesized by solid phase peptide synthesis, folded in an oxidative buffer, purified by RP-HPLC and characterized by MALDI-TOF-MS (sequence and schematic structure are shown in Figure 2). Folded peptide 3-4A recorded an m/z value of 3940.2 which corresponded to the $[M+H]^+$ (calculated m/z = 3938.6). The knottin peptide 3-4A was then site-specifically conjugated to NOTA through its N-terminal amino group using an N-hydroxysuccimide ester NOTA derivative. The resulting NOTA-3-4A showed a m/z = 4225.2 for $[MH]^+$ (calculated m/z= 4226.0). The NOTA-3-4A peptide was then radiolabeled with ^{64}Cu. The radiochemical yield of ^{64}Cu-NOTA-3-4A peptide was >70%, and radiochemical purity was > 95% as analyzed by radio-HPLC. A modest specific activity of 4.3 MBq/nmol of ^{64}Cu-NOTA-3-4A was obtained at

the end of synthesis (decay-corrected). The stability of ^{64}Cu-NOTA-3-4A was further evaluated in PBS buffer and mouse serum. As shown by the radio-HPLC analysis, ^{64}Cu-NOTA-3-4A was highly stable and there was no degradation observed in PBS or 4h incubation in mouse serum at 37 ^{o}C (Figure 3).

^{64}Cu-NOTA-3-4A PET/CT Imaging Study

The atherosclerotic lesion in the left carotid artery was clearly visible at 1 h (Figure 4A) after injection and demonstrated high contrast with low contralateral background, which persisted from 1 h to 4 h after injection (Figure 4B). PET/CT imaging also showed that relatively high kidney signal at all the imaging time points, indicating the renal clearance of the probe. Meanwhile most of the normal organs demonstrated relatively low signal. Further small animal PET quantification analysis showed that the atherosclerotic plaques uptake was 7.41 ± 1.44 %ID/g at 1 h p.i., whereas normal tissues such as common contralateral artery, brain, heart, liver and muscle exhibited much lower uptakes than atherosclerotic lesion (Figure 4C). Because of the renal clearance of the PET probe, high accumulation of ^{64}Cu-NOTA-3-4A in kidneys was observed from 1 h to 4 h, which decreased to 4.63 ± 0.54 %ID/g at 24 h p.i. Importantly, ^{64}Cu-NOTA-3-4A displayed high plaque-to-background tissue (common artery, brain, heart, muscle) ratios (Figure 4D). For example, at 1 h after injection, the plaque-to-common artery, plaque-to-brain, plaque-to-heart, plaque-to-muscle ratios of ^{64}Cu-NOTA-3-4A were 17.47 ± 3.50, 27.76 ± 4.31, 21.31 ± 3.69, and 42.99 ± 5.48, respectively. Moreover, the $\alpha_v\beta_3$ integrin-targeting specificity of ^{64}Cu-NOTA-3-4A was evaluated by the co-injection of a large amount of c(RGDyK). Significantly reduced uptake of ^{64}Cu-NOTA-3-4A by left carotid atherosclerotic lesion was

observed on PET images from 1 h to 24 h p.i. (Figure 4B).

Comparative ^{18}F-FDG PET/CT Imaging Study

The atherosclerotic lesion in the left carotid artery was visible at 0.5 h after injection and demonstrated high contrast with low contralateral background from 0.5 h to 1 h p.i. (Supporting Information). ^{18}F-FDG exhibited relatively high kidney uptake. Interestingly, despite fasting and consistent experimental protocols for all mice, the myocardial and brain uptake of ^{18}F-FDG were extremely variable. Quantification analysis showed that the accumulation of ^{18}F-FDG in the left atherosclerotic plaques was much higher than the common right carotid artery (10.47 ± 0.60 %ID/g *vs.* 2.79 ± 0.40 %ID/g at 0.5 h p.i., and 10.66 ± 1.24 %ID/g *vs.* 1.91 ± 0.45 %ID/g at 1 h p.i.). The myocardial uptake of ^{18}F-FDG was ranged from 3.65 %ID/g to 26.08 %ID/g, and the brain uptake was from 4.13 %ID/g to 32.45 %ID/g 0.5 h p.i. The kidney uptake of ^{18}F-FDG was found to be 10.02 ± 1.67 %ID/g at 0.5 h p.i. and 22.88 ± 4.67 %ID/g at 1 h p.i., respectively. The plaque-to-common artery and plaque-to-muscle ratios of ^{18}F-FDG at 1 h were 5.56 ± 1.05 and 58.67 ± 3.69, respectively.

Immunofluorescence Staining

To determine whether $\alpha_v\beta_3$ integrin expression in the carotid atherosclerotic plaques was associated with macrophage infiltration and or angiogenesis, immunohistochemical staining was performed. CD68 and CD 31 staining confirmed both the presence of macrophages and angiogenesis in atherosclerotic plaques, respectively. Moreover, CD51 and CD61 staining identified the expression integrin $\alpha_v\beta_3$ in carotid atherosclerotic plaques. The results revealed the distinct colocalization of integrin $\alpha_v\beta_3$ markers with CD68 positive macrophages (Figure 5A) and

$\alpha_v\beta_3$ integrin with vessel endothelial cells (Figure 5B).

DISCUSSION

In the clinic, ^{18}F-FDG PET has been used to detect inflammation in vulnerable atherosclerotic plaques and to select patients for vascular surgery *(12)*. However, lack of specificity hampers clinical utility of ^{18}F-FDG for cardiovascular disease. Integrin $\alpha_v\beta_3$ has been reported to be an imaging marker that is highly expressed by both plaque-associated macrophages, and activated endothelial cells, which form plaque neovasculature. Imaging integrin $\alpha_v\beta_3$ expression could therefore be a usefully noninvasive tool to predict the unstable plaques.

Radiolabeled RGD peptides are of particular interest because they specifically bind integrin $\alpha_v\beta_3$. ^{18}F-Galacto-RGD was developed to detect atherosclerotic plaques in the aorta of hypercholesterolemic mice *(13)*. Although the %ID/g in the aorta was more than 2 times higher than the residual activity in the blood of the same mice, the uptake of ^{18}F-Galacto-RGD in the aorta was only 0.24 ± 0.07 %ID/g at 2 h p.i., and the aorta-to-normal vessel wall ratio was 1.3. Further evaluation of ^{18}F-Galacto-RGD in human carotid plaques revealed a positive correlation between ^{18}F-Galacto-RGD uptake and $\alpha_v\beta_3$ expression of carotid plaques *(7)*. Moreover, ^{68}Ga-DOTA-RGD was also evaluated in the aorta of hypercholesterolemic mice and showed aorta uptake 0.90 ± 0.21 %ID/g at 1 h p.i., and the aorta/heart and aorta/blood uptake ratios were 1.8 and 1.1 at 1 h p.i., respectively *(17)*. ^{18}F-Flotegatide was also reported in a mouse model of aortic plaques. It showed aorta uptake 2.8 ± 0.4 %ID/g at 1 h p.i., and the aorta-to-heart ratio and aorta-to-muscle ratio were 14 and 18, respectively *(18)*.

For the current study, to the best of our knowledge, it is the first report to describe the PET labeled knottin for imaging carotid atherosclerotic lesions. Several cystine-knot peptides, including Ecballium elaterium trypsin inhibitor (EETI-II) *(21)* and Agouti-related protein (AgRP) *(30)*, have been used as scaffolds to engineer peptides that bind integrin receptors with low nanomolar affinities. EETI-II and AgRP-based cystine peptides are small (3-4 kDa), amenable to amino acid substitutions, and have high chemical, thermal, and proteolytic stability. In our previous studies, divalent knottin 3-4A was successfully radiolabeled with ^{64}Cu *(25)* and ^{18}F *(31)* for imaging integrin $\alpha_v\beta_3$ positive U87MG tumor in living animals. In this study, PET/CT imaging and quantification results demonstrated that the atherosclerotic lesion in the left carotid artery to be clearly visible at 1 h p.i. Compared to the uninjured contralateral common carotid artery (0.67 ± 0.23 %ID/g at 1 h p.i.), the uptake of the left carotid atherosclerotic lesion was 7.41 ± 1.44 %ID/g, which was significantly higher than uptake values of ^{18}F-Galacto-RGD, ^{68}Ga-DOTA-RGD and ^{18}F-Flotegatide (P<0.05). Plaque-to-background tissue ratios especially plaque-to-heart ratio is clinically important due to the potentially debilitating effects of myocardial infarctions. Compared to the previously reported RGD based PET probes, ^{64}Cu-NOTA-3-4A also displayed much higher plaque-to-heart ratio (27.8 at 1h p.i.). Considering there is no huge difference for the αvβ3 in vitro affinity of the ^{18}F-Galacto-RGD, DOTA-RGD and DOTA-3-4A (5, 3.2 and 8 nM, respectively) (*13, 17, 25*), the different imaging results among these probes is very likely caused by their different in vivo pharmacokinetic properties of the probes.

Comparisons to ^{18}F-FDG PET are also presented here. The atherosclerotic lesion in the left

carotid artery was readily visible at 0.5 h after injection of ^{18}F-FDG. Although the accumulation of ^{18}F-FDG by plaques was higher than that of ^{64}Cu-NOTA-3-4A at 1 h p.i. (10.66 ± 1.24 %ID/g *vs.* 7.41 ± 1.44 %ID/g, $P<0.05$), the plaque-to-common carotid artery ratio of ^{18}F-FDG was significantly lower than that of ^{64}Cu-NOTA-3-4A at 1 h p.i. (3.75 *vs.* 14.71, $P<0.05$). The normal myocardial and brain uptake of ^{18}F-FDG in mice was extremely variable and the ratios of plaque-to-brain and plaque-to-heart were difficult to be exactly evaluated. Thus, ^{18}F-FDG imaging of atherosclerotic plaques in brain and heart arteries may be of limited clinical utility. Compared with ^{18}F-FDG, ^{64}Cu-NOTA-3-4A did not accumulate in normal myocardium and brain, which could be beneficial for imaging coronary and brain vessels. In addition, successful use of ^{64}Cu-DOTATATE in human neuroendocrine tumors highlights the promise of ^{64}Cu based probes in clinical settings *(32)*. Similarly, ^{64}Cu-NOTA-3-4A may potentially be used to image a variety of integrin $\alpha_v\beta_3$ positive lesions in human subjects. A variety of engineered cystine-knot peptides coupled to different PET labels are undergoing extensive testing and validation *(22, 26, 31)*.

Finally, the immunofluorescent staining displayed a correlation between integrin $\alpha_v\beta_3$ expression and macrophage infiltration, as well as formation of the neovasculature. These data indicate that the uptake mechanism of ^{64}Cu-NOTA-3-4A by atherosclerotic plaques is through binding to integrin $\alpha_v\beta_3$ expressed on the surface of macrophages and endothelial cells.

CONCLUSION

^{64}Cu-NOTA-3-4A displayed significantly high and specific accumulation in carotid atherosclerotic plaques, which correlated by immunofluorescence staining to overexpression $\alpha_v\beta_3$

integrin by both macrophages and angiogenic endothelial cells. Moreover, lower normal tissues uptake of ^{64}Cu-NOTA-3-4A and a high plaque-to-normal tissue ratios were observed. Collectively, these results suggest that ^{64}Cu-NOTA-3-4A may be a promising PET probe for clinical imaging of carotid atherosclerotic plaques.

ACKNOWLEDGEMENTS

This work was supported, in part, by the Office of Science (BER), U.S. Department of Energy (DE-SC0008397), NIH In Vivo Cellular Molecular Imaging Center (ICMIC) grant P50 CA114747, and National Science Foundation for Young Scholars of China (Grant No. 81101072).

REFERENCES

1. Libby P. Inflammation in atherosclerosis. *Nature*. 2002;420:868-874.
2. Libby P, Ridker PM, Maseri A. Inflammation and atherosclerosis. *Circulation*. 2002;105:1135-1143.
3. Narula J, Garg P, Achenbach S, Motoyama S, Virmani R, Strauss HW. Arithmetic of vulnerable plaques for noninvasive imaging. *Nat Clin Pract Cardiovasc Med*. 2008;5:S2-S10.
4. Saraste A, Nekolla SG, Schwaiger M. Cardiovascular molecular imaging: an overview. *Cardiovasc Res*. 2009;83:643-652.
5. Gerretsen S, Kessels AG, Nelemans PJ, et al. Detection of coronary plaques using MR coronary vessel wall imaging: validation of findings with intravascular ultrasound. *Eur Radiol*. 2013;23:115-124.
6. Huang PT, Huang FG, Zou CP, et al.Contrast-enhanced sonographic characteristics of neovascularization in carotid atherosclerotic plaques. *J Clin Ultrasound.* 2008;36:346-351.
7. Beer AJ, Pelisek J, Heider P, et al. PET/CT imaging of integrin alphavbeta3 expression in human carotid atherosclerosis. *JACC Cardiovasc Imaging*. 2014;7:178-187.
8. Ogawa M, Magata Y, Kato T, et al. Application of 18F-FDG PET for monitoring the therapeutic effect of antiinflammatory drugs on stabilization of vulnerable atherosclerotic plaques. *J Nucl Med*. 2006;47:1845-1850.
9. Tahara N, Kai H, Ishibashi M, et al. Simvastatin attenuates plaque inflammation: evaluation by fluorodeoxyglucose positron emission tomography. *J Am Coll Cardiol*.

2006;48:1825-1831.

10. Rudd JH, Warburton EA, Fryer TD, et al. Imaging atherosclerotic plaque inflammation with [18F]-fluorodeoxyglucose positron emission tomography. *Circulation*. 2002;105:2708-2711.
11. Tawakol A, Migrino RQ, Bashian GG, et al. In vivo 18F-fluorodeoxyglucose positron emission tomography imaging provides a noninvasive measure of carotid plaque inflammation in patients. *J Am Coll Cardiol*. 2006;48:1818-1824.
12. Pedersen SF, Graebe M, Hag AM, Hoejgaard L, Sillesen H, Kjaer A. Microvessel density but not neoangiogenesis is associated with 18F-FDG uptake in human atherosclerotic carotid plaques. *Mol Imaging Biol*. 2012;14:384-392.
13. Laitinen I, Saraste A, Weidl E, et al. Evaluation of alphavbeta3 integrin-targeted positron emission tomography tracer 18F-galacto-RGD for imaging of vascular inflammation in atherosclerotic mice. *Circ Cardiovasc Imaging*. 2009;2:331-338.
14. Yao Y, Jiang Y, Sheng Z, et al. Analysis of in situ and ex vivo alphaVbeta3 integrin expression during experimental carotid atherogenesis. *Int J Nanomedicine*. 2012;7:641-649.
15. Waldeck J, Hager F, Holtke C, et al. Fluorescence reflectance imaging of macrophage-rich atherosclerotic plaques using an alphavbeta3 integrin-targeted fluorochrome. *J Nucl Med*. 2008;49:1845-1851.
16. Wu W, Wang Y, Shen S, et al. In vivo ultrasound molecular imaging of inflammatory thrombosis in arteries with cyclic Arg-Gly-Asp-modified microbubbles targeted to glycoprotein IIb/IIIa. *Invest Radiol*. 2013;48:803-812.
17. Johanna H, Iina L, Pauliina L, et al. 68Ga-DOTA-RGD peptide: biodistribution and binding

into atherosclerotic plaques in mice. *Eur J Nucl Med Mol Imaging*. 2009;36:2058-2067.

18. Su H, Gorodny N, Gomez LF, et al. Atherosclerotic plaque uptake of a novel integrin tracer F-Flotegatide in a mouse model of atherosclerosis. *J Nucl Cardiol*. 2014;21:553-562.
19. Burtea C, Laurent S, Murariu O, et al. Molecular imaging of alpha v beta3 integrin expression in atherosclerotic plaques with a mimetic of RGD peptide grafted to Gd-DTPA. *Cardiovasc Res*. 2008;78:148-157.
20. Saraste A, Laitinen I, Weidl E, et al. Diet intervention reduces uptake of alphavbeta3 integrin-targeted PET tracer 18F-galacto-RGD in mouse atherosclerotic plaques. *J Nucl Cardiol*. 2012;19:775-784.
21. Kimura RH, Cheng Z, Gambhir SS, Cochran JR. Engineered knottin peptides: a new class of agents for imaging integrin expression in living subjects. *Cancer Res*. 2009;69:2435-2442.
22. Miao Z, Ren G, Liu H, et al. An engineered knottin peptide labeled with 18F for PET imaging of integrin expression. *Bioconjug Chem*. 2009;20:2342-2347.
23. Jiang L, Kimura RH, Miao Z, et al. Evaluation of a (64)Cu-labeled cystine-knot peptide based on agouti-related protein for PET of tumors expressing alphavbeta3 integrin. *J Nucl Med*. 2010;51:251-258.
24. Jiang L, Miao Z, Kimura RH, et al. Preliminary evaluation of (177)Lu-labeled knottin peptides for integrin receptor-targeted radionuclide therapy. *Eur J Nucl Med Mol Imaging*. 2011;38:613-622.
25. Kimura RH, Jones DS, Jiang L, Miao Z, Cheng Z, Cochran JR. Functional mutation of multiple solvent-exposed loops in the Ecballium elaterium trypsin inhibitor-II cystine knot

miniprotein. *PLoS ONE*. 2011;6:e16112.

26. Liu S, Liu H, Ren G, Kimura RH, Cochran JR, Cheng Z. PET Imaging of Integrin Positive Tumors Using F Labeled Knottin Peptides. *Theranostics*. 2011;1:403-412.
27. Jiang L, Miao Z, Kimura RH, et al. 111In-labeled cystine-knot peptides based on the Agouti-related protein for targeting tumor angiogenesis. *J Biomed Biotechnol*. 2012;2012:368075.
28. Jiang H, Moore SJ, Liu S, et al. A novel radiofluorinated agouti-related protein for tumor angiogenesis imaging. *Amino Acids*. 2013;44:673-681.
29. Natarajan A, Habte F, Liu H, et al. Evaluation of Zr-rituximab tracer by cerenkov luminescence imaging and correlation with PET in a humanized transgenic mouse model to image NHL. *Mol Imaging Biol*.2013;15:468-475.
30. Silverman AP, Levin AM, Lahti JL, Cochran JR. Engineered cystine-knot peptides that bind alpha(v)beta(3) integrin with antibody-like affinities. *J Mol Biol*. 2009; 385:1064-1075.
31. Jiang L, Kimura RH, Ma X, et al. A radiofluorinated divalent cystine knot peptide for tumor PET imaging. *Mol Pharmacol*. 2014;11:3885-3892.
32. Pfeifer A, Knigge U, Mortensen J, et al. Clinical PET of neuroendocrine tumors using 64Cu-DOTATATE: first-in-humans study. *J Nucl Med*. 2012; 53:1207-1215.

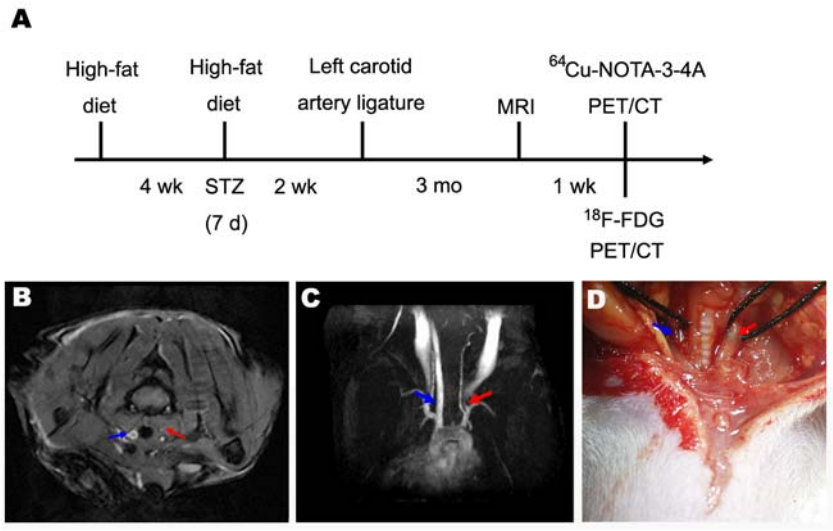

FIGURE 1. A: Study design diagram. B and C: MRI images of the vessel of carotid atherosclerotic plaques (red arrow) and the control (blue arrow). D: The bright field anatomic image of the vessel with carotid atherosclerotic plaques (red arrow) and the control (blue arrow).

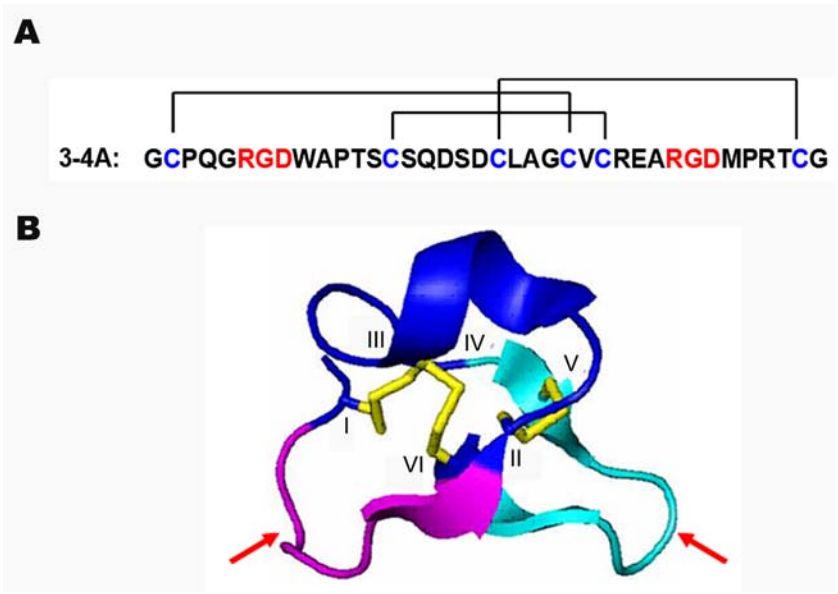

FIGURE 2. A: Peptide sequences of EETI mutant 3-4A, and black lines represent the disulfide bonds between Cys^1-Cys^4, Cys^2-Cys^5, and Cys^3-Cys^6. B: Schematic of 3-4A. Yellow lines represent disulfide bonds between cystines (I-VI). Purple loop and light blue loop (Red arrows) are engineered to contain a RGD motif, respectively.

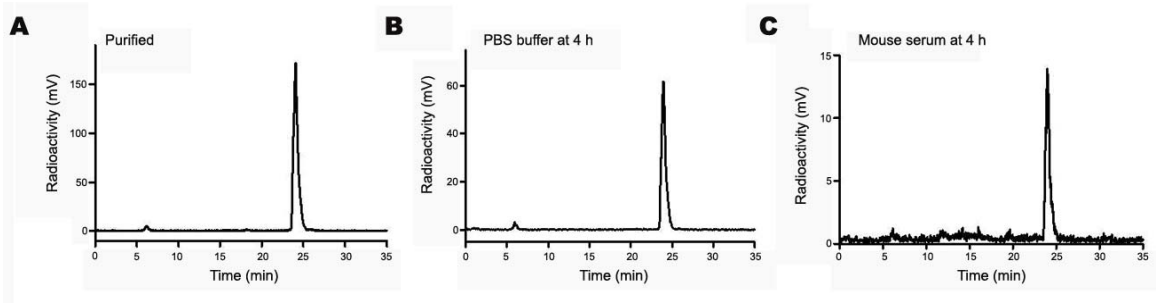

FIGURE 3. Stability analysis of ^{64}Cu-NOTA-3-4A (A) in PBS buffer (B) at room temperature and mouse serum (C) at 37 ^{o}C for 4 h, respectively.

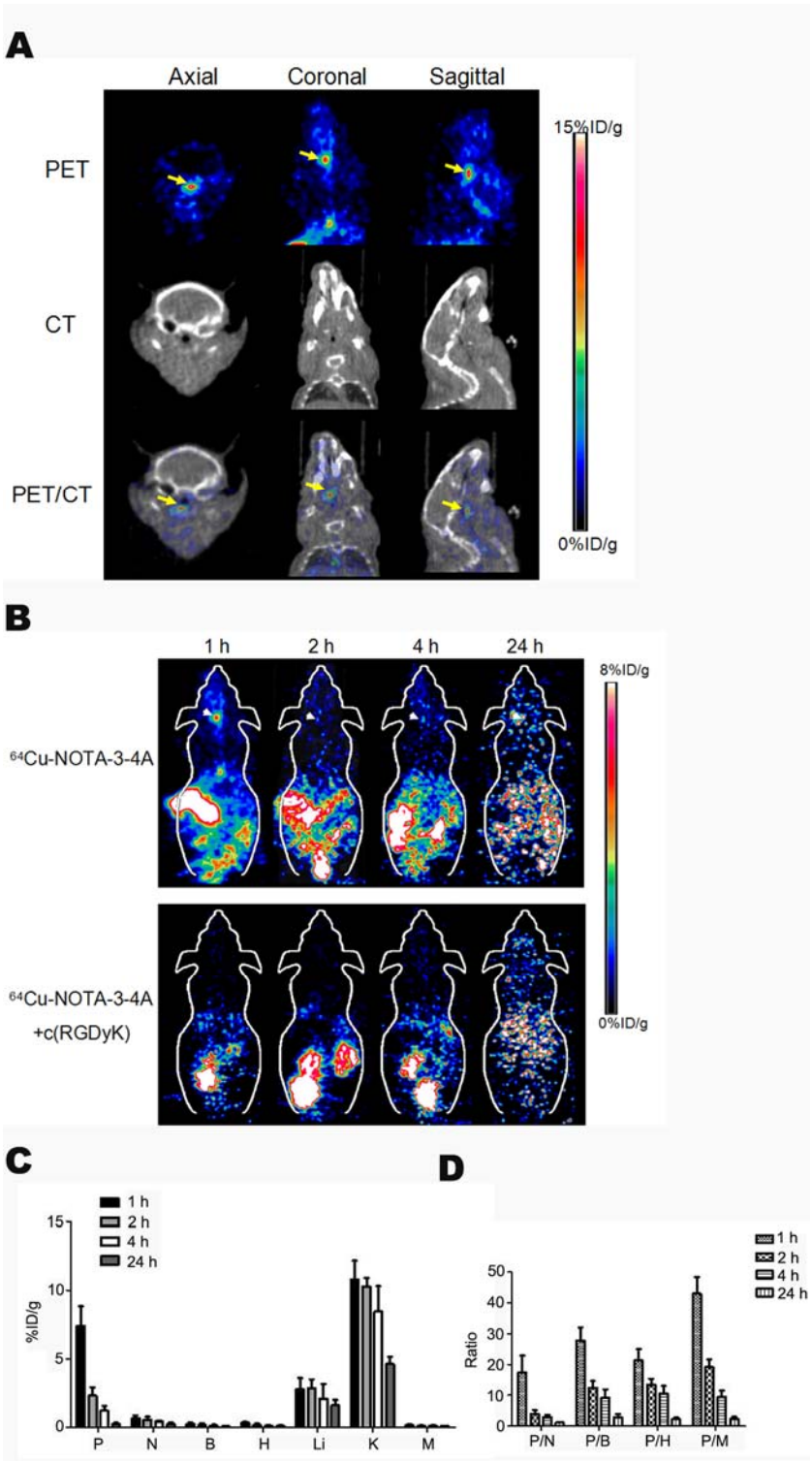

FIGURE 4. Small animal PET images and quantification analysis results of ^{64}Cu-NOTA-3-4A. A: PET, CT and PET/CT images of mice models with carotid atherosclerotic plaques at 1 h p.i. of

^{64}Cu-NOTA-3-4A. B: Coronal PET images of mice models with carotid atherosclerotic plaques at 1, 2, 4 and 24 h p.i. of ^{64}Cu-NOTA-3-4A without or with c(RGDyK). C: Quantification analysis of radioactivity accumulation in selected organs at different time points p.i. of ^{64}Cu-NOTA-3-4A, reported as %ID/g (P: plaque, N: normal vessel wall, B: blood, H: heart, Li: liver, K: kidney, M: muscle). D: Quantification analysis of plaque-to-normal tissues ratios at different time points.

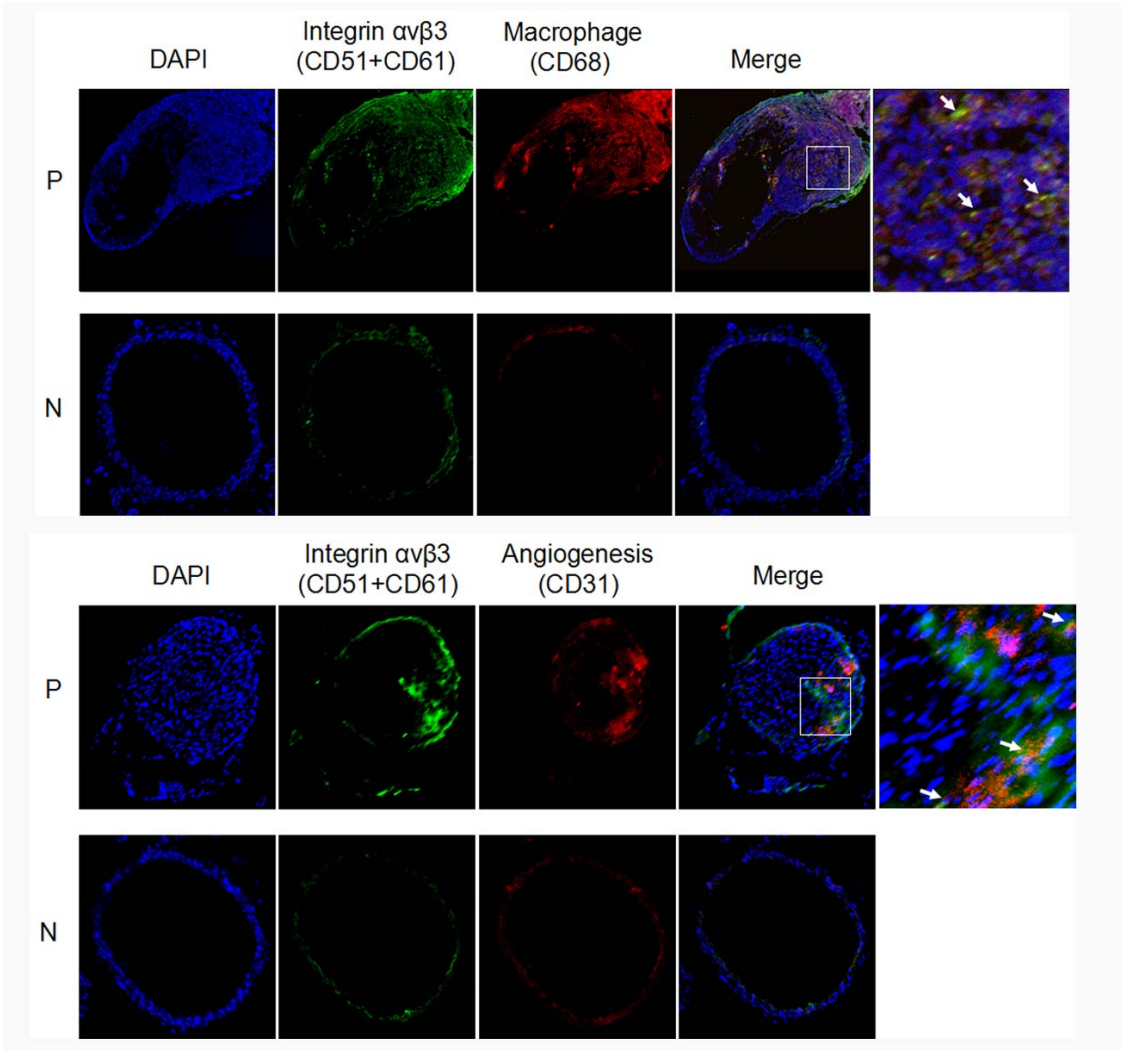

FIGURE 5. Immunofluorescent result of carotid atherosclerotic plaques.